Separation and Purification Technology 368 (2025) 133016

Contents lists available at ScienceDirect

Separation and Purification Technology

journal homepage: www.elsevier.com/locate/seppur

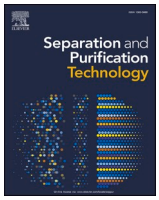

Reservoir effect of Nano-Porous carbon for enhancing Anti-Deactivation of anatase nanocrystal towards photocatalytic oxidation of toluene

Weiping Zhang [a,b,*], Haiyong Pan [a,b], Yuqing Huang [a,b], Xian Xia [a,b], Hongli Liu [a,b], Weina Zhao [a,b], Jiejing Kong [a,b], Yanrong Zhang [c], Taicheng An [a,b]

[a] Guangdong Key Laboratory of Environmental Catalysis and Health Risk Control, Guangdong-Hong Kong-Macao Joint Laboratory for Contaminants Exposure and Health, Institute of Environmental and Chemical Engineering Innovation, Institute of Environmental Health and Pollution Control, Guangdong University of Technology, Guangzhou 510006, China

[b] National Engineering Laboratory for VOCs Pollution Control Material & Technology Guangdong Branch, Guangdong Basic Research Center of Excellence for Ecological Security and Green Development, Guangdong Engineering Technology Research Centre for Photocatalytic Technology Integration and Equipment, School of Environmental Science and Engineering, Guangdong University of Technology, Guangzhou 510006, China

[c] School of Environmental Science and Engineering, Huazhong University of Science and Technology, Wuhan 430074, China

ARTICLE INFO

Editor: Jorge Bedia

Keywords:
VOC
Photocatalytic oxidation
Anti-deactivation
Synergetic effect
Core–shell

ABSTRACT

The incomplete oxidation of VOCs often leads to the formation of nonvolatile carbonaceous species on anatase photocatalyst. It is still a challenge to solve the photocatalysts deactivation due to the accumulation of carbonaceous species. In the present contribution, we successfully revealed the anti-deactivation mechanism towards photocatalytic oxidation of toluene in an NPC@TiO_2 photocatalyst. By introducing nano-carbon core into anatase TiO_2 nanocrystal, the carbon core can be used as a temporary reservoir for toluene and lone electrons to enhance selective adsorption of toluene and charge separation, sequentially elevating mass transfer and oxidation reaction at multiple interfaces of photocatalyst. The pre-trapped toluene can be attacked directly in the effect of oxidation radicals formed at the interfaces without engendering excessive carbonaceous species, significantly facilitating the degradation and mineralization of toluene. Meanwhile, avoiding the saturated adsorption of toluene on the photocatalyst is a critical element to maintain their stable photocatalytic activity. Our research introduces an efficient deep oxidation strategy that is enabled by subtle control of the adsorption-conversion of VOCs on a multi-interface structure.

Environmental Implication.

The incomplete oxidation of VOCs and accumulation of carbonaceous species often lead to photocatalyst deactivation. This severely limits the application of photocatalysts in industrial VOCs waste gas treatment. By introducing nano-carbon core into anatase TiO_2 nanocrystal, nano-porous carbon can act as a temporary reservoir of VOC molecular and lone electrons to enhance the selective adsorption trapping of VOC and the separation of photogenerated carrier, thereby avoid the deactivation of photocatalyst. This is of great significance for the design of highly efficient and stable photocatalysts by optimizing active sites of adsorption and reaction for the deep oxidation of VOCs.

1. Introduction

Aromatic volatile organic compounds (VOCs) are commonly used as industrial raw materials and solvents, making them a significant component of industrial VOC emissions. Toluene, a ubiquitous VOC, has aroused extensive attention for its significant hazard to the environment (such as formation of ozone, SOAs etc.) and health (such respiratory illnesses and chronic poisoning), even in an infinitesimal concentration [1,2]. Therefore, selecting a stable and efficient display technology for the removal of toluene is of paramount importance. In this respect, photocatalytic oxidation technology has been recognized as an efficient strategy for the removal of toluene in an economy for energy and environmentally friendly manner, especially by purifying and detoxifying the waste gas of VOCs with low concentration[3–5].

Although considerable research has been devoted to investigating the enhancement of toluene degradation, it is still a challenge to reveal

* Corresponding author.
E-mail address: wp.zhang86@gdut.edu.cn (W. Zhang).

https://doi.org/10.1016/j.seppur.2025.133016
Received 6 March 2025; Received in revised form 8 April 2025; Accepted 13 April 2025
Available online 14 April 2025

the deep oxidation mechanism at the interfaces of photocatalyst[6–8]. In general, toluene oxidation reaction is closely related to their residence time and the concentration of radical species on the interfaces, which is regarded as the critical factors toward toluene removal in photocatalysis [9,10]. Due to the disordered reaction, massive and diverse uphill reactions are corroborated during toluene degradation process, while the competitive adsorption and reaction between the numerously generated intermediate species and toluene, subsequently encountering a low degradation and mineralization[3,11–13]. Therefore, exploring and tailoring a more efficient mass transfer-reaction strategy will be one of prominent significance for the photocatalytic elimination of toluene.

Anatase titanium dioxide (TiO_2), due to its advantages such as strong oxidative ability, has been intensively investigated in the field of VOCs emission control[14–16]. However, due to its inherent defects, such as high recombination of photogenerated electron/hole and low VOCs capture efficiency, TiO_2 commonly suffers the rapid deactivation for VOCs elimination, which is attributed to the accumulation of carbonaceous intermediates[17–19]. These refractory intermediates such carbonaceous polymers, chlorine, nitrate, sulfate and etc. were tightly adsorbed onto the interface of anatase TiO_2, which will increased the competitive adsorption-reaction with reaction substrate[20–22]. What's more, because the strong interaction between the intermediates and photocatalyst and the scarcity of radical species hinder the removal of carbonaceous intermediates in time, the active sites of the photocatalyst are occupied by the intermediates, thus encountering the performance retardation[6,8,23]. As a result, avoiding the intermediates accumulation at the reactive interface is the key to developing a photocatalyst with high durability and efficiency for VOCs purification.

Nano-porous carbon (NPC) has been confirmed to be a temporary reservoir with excellent VOCs adsorption affinity and electroconductivity towards resistance of carbonaceous intermediates and coke deposition in our previous works[6,14,24]. Intriguingly, coupling these materials with anatase TiO_2 can effectively shorten the mass transfer-reaction time and enhance the concentration of oxygen free radicals at photocatalyst interface, thus greatly reducing the formation and accumulation of non-volatile oxygen-containing intermediates[10,25]. Hence, NPC is considered as a highly efficient additive of anatase TiO_2-based photocatalyst in VOCs control. However, it is still a difficult problem to obtain composite photocatalysts with high CO_2 selective conversion by regulating the TiO_2/NPC composite interface structure at the microscopic scale, especially in the synergistic anti-deactivation mechanism of porous carbon and anatase TiO_2 at the molecular scale.

In this study, we successfully tailored adsorption-mass transfer model and reaction pathway of toluene removal by introducing nano-carbon core into anatase TiO_2 shell, where the carbon core can be used as a temporary reservoir for toluene and lone electrons to elevate the mass transfer and oxidation reaction of toluene at multiple interfaces of photocatalyst. Experimental results revealed that the delocalized electrons of nano-carbon core were favorable for facilitating photogenerated charge separation and the formation of reactive oxygen species. Furthermore, the pre-trapped toluene can be attacked directly in the effect of oxygen radicals formed at the interface without engendering excessive carbonaceous species, significantly facilitating the degradation and mineralization of toluene. This work will provide new strategies and ideas to solve the photocatalyst deactivation problem involved in purification of VOCs.

2. Experimental section

2.1. Synthesis of NPC@TiO_2

The nano-porous carbon decorated TiO_2 nanocrystal (NPC@TiO_2) samples were prepared by a pyrolysis and activation method. Firstly, hydrothermal carbon sphere (HTCS) template was synthesized by our previous method[26]. Amount of HTCS was mixed with 0.18 g SDS, 629 μ L 2 M $TiCl_4$ and 70 mL ethanol water solution ($V_{ethanol/water}$ = 3:4). After 30 min ultrasonic treatment, 10 mL of urea aqueous solution (containing 0.42 g urea) was slowly added to the solution drop by drop and stirred at 53 °C for 24 h. The obtained precursor was freeze-dried and then put into a tube furnace. The precursor was maintained at 500 °C for 240 min at a heating rate of 5 °C/min with Ar gas protection. Finally, the precursor was placed into a muffle furnace, and activated at 200–600 °C for 60 min at a heating rate of 1 °C/min to obtain NPC@TiO_2, which defined as NPC@TiO_2-200, NPC@TiO_2-300, NPC@TiO_2-400, NPC@TiO_2-500, NPC@TiO_2-600, respectively. The details of characterization of photocatalysts can be seen **Supporting Information (SI)**.

2.2. Photocatalytic performance for gas toluene removal

Photocatalytic removal of gaseous toluene was performed in a photocatalytic reaction system equipped with a gas distribution (Zhongjiaojinyuan Science and Technology Co. Ltd., China). Stable and continuous gaseous toluene with a concentration of 40 ± 1ppmv was obtained before photocatalytic reaction. 80 mg of synthesized powder was filled into a customized cubic quartz glass reactor (2.5 cm × 1.0 cm × 0.15 cm) with a 300 W xenon lamp as the light source. Before irradiation, the adsorption of gas toluene on the photocatalyst reached equilibrium. The automatic feeding device was used to sample the gas at a certain interval, and the concentration of toluene and CO_2 was determined by gas chromatography equipped with a nickel reforming furnace (Shanghai Kechuang Chromatography Instrument Co., LTD., China). As compared, the toluene-adsorption tests and photocatalytic reaction without toluene pre-adsorption were also performed to determine the adsorption capacity and photocatalytic performance of the photocatalysts (the detail seen in the **SI**).

2.3. In situ DRIFTS analysis

The adsorption and reaction changes of toluene on catalyst interface were characterized by in-situ Diffuse Reflectance Infrared Fourier Transform Spectroscopy (DRIFTS). After 20 min of nitrogen purging to remove gases from the reactor chamber, the sample was heated to 150 °C and subjected to a 60 min pretreatment. When the temperature was cooled to the 30 °C, the baseline collection was performed, and the reactive gas of toluene was transferred to the reaction chamber. At this point, the catalyst surface after adsorption of toluene was used to collect the background, and simulated sunlight was introduced to collect the infrared information on the photocatalyst surface every 10 min. As compared, the in-situ DRIFTS of toluene adsorption on photocatalyst without simulated sunlight was also performed.

2.4. Carbonaceous intermediates Identification

80 mg of used-photocatalyst was transferred into a 100 mL of conical flask with 60 mL methanol and disposed under ultrasonic condition for 30 min. The obtained suspension was filtered, and the mixed extract was concentrated to 1 mL by a rotary evaporator, and then completely dried with a gentle stream of high-purity nitrogen. The sample was redissolved in 1 mL ethyl acetate and then injected into the gas chromatograph (Agilent 7890B) coupled with a mass selective detector (Agilent 5977B) (GC–MSD) with a HP-5 ms column (30 m × 0.25 mm × 0.25 μm film thickness). The carbonaceous species were also determined by XPS semiquantitative method and thermogravimetry analysis (TGA).

2.5. DFT calculation

Gaussian structure optimization is first performed, followed by the calculation of adsorption energy using the Dmol3 module in Materials Studio. In the parameterization of the Perdew–Burke–Ernzerhof (PBE) functional, all density functional theory (DFT) calculations are conducted using the generalized gradient approximation (GGA). The

dispersion-corrected DFT-D2 method is employed to calculate hydrogen bonds, van der Waals, and other weak interactions. A set of numerical Kohn-Sham atomic orbitals is augmented with a double numeric basis set with polarization functions (DNP)[24,27]. The convergence criteria for structural optimization and energy calculation parameters are as follows: (a) energy tolerance of 1.0×10^{-5} Ha, (b) maximum force tolerance of 2.0×10^{-3} Ha/Å, (c) maximum displacement tolerance of 5.0×10^{-3} Å. The SCF electronic self-consistent iteration calculation convergence criterion is 1.0×10^{-6}, with a maximum cycle number of 500 times, and the maximum step length for each optimization of atomic movement is 0.3 Å. The adsorption energy can be calculated according to the following equation:

$E_{ads} = E_{A\text{-}B}\text{-}E_A\text{-}E_B$.

Where $E_{A\text{-}B}$ refers to the energy of system AB after substance A is adsorbed on substrate B. E_A represents the energy of substance A, and E_B represents the energy of substrate B.

3. Results and discussions

3.1. Morphology, structure, and composition analysis

Toluene can be hardly captured and mineralized by close-packed or agglomerate TiO_2 photocatalysts due to their fewer exposure adsorption sites and lower oxidation efficiency[28,29]. Based on this, the photocatalysts of nano-porous carbon decorated TiO_2 nano-shells were fabricated by a dip adsorption-activation method using HTCS (composed of amorphous ultrafine polymeric carbon) as a template, and the TEM images of NPC@TiO_2-200 associated with interfacial structure and composition were shown in Fig. 1. TiO_2 nano-shell is tightly coated on the nano-porous carbon core to form a tight nano-spherical composite structure with an obvious boundary between the spherical particles (Fig. 1a). Due to the structural-directing effect of ultrafine polymeric carbon, the superfine TiO_2 nanocrystals are formed at the carbon core interface. It is observed that the exposed morphology of TiO_2 nanocrystals becomes more obvious at the composite interface with the increase of activation temperature (See SI in Fig. S1). When the activation temperature reaches 500 °C, the nano-carbon core almost disappears, and the shell size obviously thickens and shrinks. Furthermore, a selected area electron diffraction (SAED) pattern was taken from the NPC@TiO_2-200 composite interface (bottom right inset in Fig. 1b), corresponding to polycrystal anatase, which indicated that TiO_2 nano-shell was composed of anatase TiO_2 nanocrystals in different directions. HR-TEM image (Fig. 1c) showed that the TiO_2 are highly crystallized and composed of many nanocrystals, as evidenced by the well resolved TiO_2 (101) (0.343 nm) crystalline lattices[30,31]. Meanwhile, EDX mapping results showed that Ti and O species in the electronic image were uniformly dispersed on the nano carbon core (Fig. 1d2 ~ d_4), and the well-distributed oxidation components would be beneficial for toluene capture and charge transfer due to the organic affinity and uniform composite interface[32,33].

The XRD patterns of as-prepared sample are given in Fig. 2a. It is noted that as-prepared samples present anatase characteristics of 101 (25.28°), 004 (37.84°), 200 (48.12°), 105 (53.89°), 211 (55.03°), 213 (62.40°), 204 (62.85°), 116 (68.74°), 220 (70.38°) and 215 (75.08°) crystal planes (PDF#21–1272), 101 of them are highly exposed crystal faces[34,35]. The peaks observed at 26–28° can be attributed to the (110) crystallographic plane of the rutile phase, which can be attributed to the local phase transition of anatase TiO_2 due to the presence of carbon components. Moreover, the obtained NPC@TiO_2-200 shows the lowest peak intensity, which can be attributed to the steric hindrance effect of nano-porous carbon inhibiting the growth of TiO_2 nanocrystals, resulting in a small exposure size (See SI in Table S1). With increasing the activation temperature, small size nanocrystals gradually agglomerate and form larger size nanoparticles with higher diffraction intensity, these results are very consistent with TEM analysis results. XPS measurements were employed to further obtain information on the surface chemical composition, oxidation states, and bonding configuration of the obtained NPC@TiO_2 sample (See SI in Fig. S2). The Ti 2p, O 1 s and C 1 s appeared in the composite, which confirmed the usefulness of the preparation method. Thereinto, O 1 s (See SI in Fig. S2b) were separated into peaks at 533.8, 532.6, 531.6, and 530.3 eV, corresponding to O-C=O, C-O-C, C=O, and Ti-O, respectively, and C 1 s (See SI in Fig. S2c) were separated into peaks at 289.1, 287.2, 286.1, and 284.8 eV, corresponding to O-C=O, C-OH, C–C and C=C, respectively

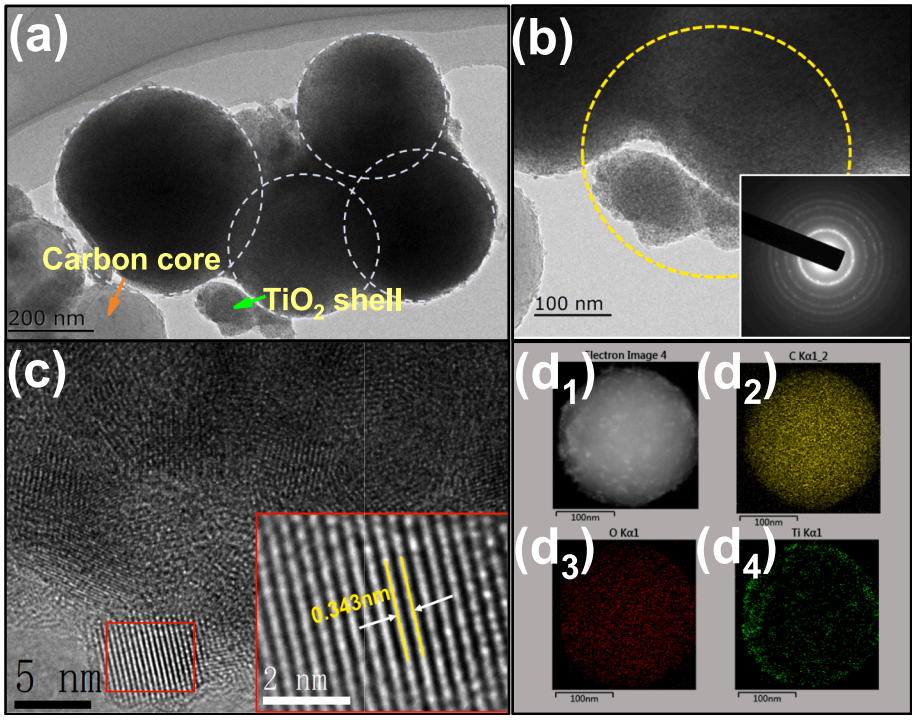

Fig. 1. TEM image (a), SAED pattern (b), HR-TEM image (c) and EDX mapping (d) of as prepared NPC@TiO_2-200.

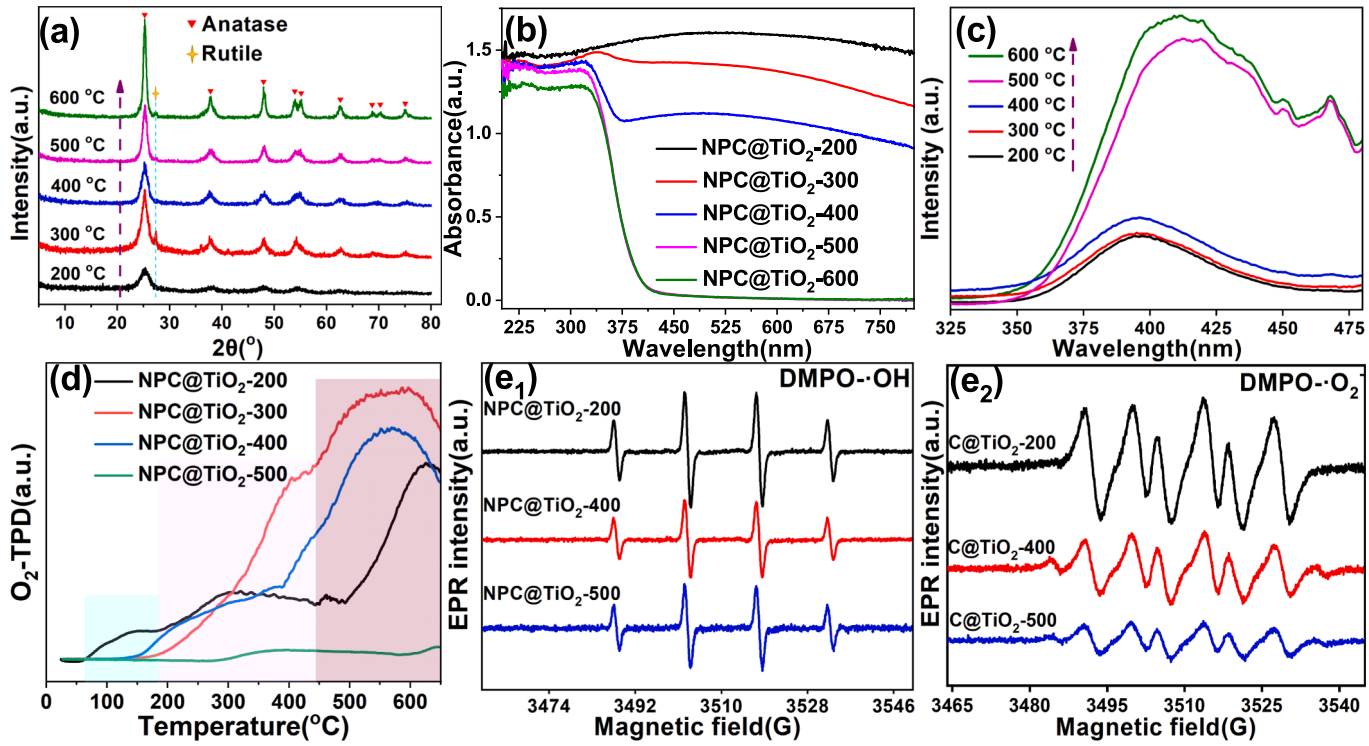

Fig. 2. XRD patterns (a), UV–vis spectra (b), PL spectra (c), and O_2-TPD curves (d) of NPC@TiO_2. EPR spectra (e) of DMPO-•OH (e_1) and DMPO-•O_2^- (e_2) under simulated sunlight of NPC@TiO_2.

[14,24,36]. Combined with the above TEM analysis, these results indicated a tight heterogeneous interface could be formed between TiO_2 and nano-porous carbon, which would be beneficial for the interfacial charge transfer and mass transfer[14,37].

The UV − vis diffuse reflectance spectrum (Fig. 2b) was employed again to distinguish the light harvest capacity. NPC@TiO_2-200 performed a strengthen light harvest ability because of its higher carbon content (See SI in Fig. S3). Meanwhile, the nano-porous carbon component (NPC@TiO_2-200, 55.41 % > NPC@TiO_2-300, 45.01 % > NPC@TiO_2-400, 25.68 % > NPC@TiO_2-500, 1.97 % > NPC@TiO_2-600, 1.24 %) in NPC@TiO_2 was significantly decreased with increasing the activated temperature, resulting in lower adsorption intensity of NPC@TiO_2 with high activated temperature (See SI in Fig. S3a-e). The enhancement of the light absorption threshold was attributed to the increased conjugated or non-conjugated structures of nano-porous carbon, which was sequentially responsible for the increase of n → π* or π → π* [3,38,39]. To understand the migration and recombination of photogenerated e^-/h^+ pairs, the fluorescence properties of the photocatalysts were also carefully discussed (Fig. 2c). The results showed that NPC@TiO_2-200 exhibited a lower PL intensity near 395 nm than that of other composites, indicating that the photogenerated carrier separation of samples with high nano-porous carbon content were faster than that of samples with low nano-porous carbon content, which were mainly attributed to the effective electron migration characteristics between nano-porous carbon and TiO_2 nanocrystal[40]. Photoelectrochemical characterization (including photocurrent response and EIS analysis) further confirms that the synergistic effect between nano-porous carbon and ultrasmall TiO_2 nanocrystals significantly enhances interfacial charge transfer and separation efficiency (Fig. S4). Apparently, nano-porous carbon played an important role in the process of light absorption and photogenerated carrier separation.

It is well known that oxygen storage capacity is another important index of photocatalyst performance because the adsorbed molecular O_2 can be activated and transformed into superoxide radicals (•O_2^-). Herein, a O_2 temperature-programmed desorption (O_2-TPD) was conducted to verify the oxygen storage capacity of NPC@TiO_2 composites and shown in Fig. 2d. Two O_2 desorption peaks were observed over the NPC@TiO_2-200 composite, which were assigned to molecularly adsorbed oxygen O_2^- (range from 56 to 300 °C) and surface chemically adsorbed oxygen O^- (range from 300 to 500 °C). The desorption peak of molecular oxygen for NPC@TiO_2-200 is higher than other NPC@TiO_2 samples, indicating that NPC@TiO_2-200 possesses more active sites for molecular oxygen adsorption. Since photocatalytic reactions typically occur at relatively low temperatures (<100 °C) and superoxide radicals (•O_2^-) are primarily derived from the conversion of molecular oxygen, NPC@TiO_2-200 exhibits superior photocatalytic performance compared to other NPC@TiO_2 photocatalysts [14,41].

Reactive oxygen species (ROS) were supposed to be all-important during photocatalytic oxidation of VOCs. Herein, EPR was employed to detect hydroxyl radicals (•OH) and superoxide radicals (•O_2^-). Strong EPR signals of DMPO–•OH (Fig. 2e1) and DMPO–•O_2^- (Fig. 2e2) adducts are observed in three NPC@TiO_2 photocatalyst under stimulated solar light irradiation, suggesting that •OH and •O_2^- are the important ROS in this system [20]. Moreover, the EPR intensity of DMPO–•OH and DMPO–•O_2^- over NPC@TiO_2-200 is much higher than that of NPC@TiO_2-400 and NPC@TiO_2-500, which indicates that the effective electron acceptor of nano-porous carbon in NPC@TiO_2-200 could effectively promote the rapid transfer of separated carriers, and subsequently react with OH^- and adsorbed oxygen to form •OH and •O_2^-. These results are very consistent with PL and O_2-TPD results.

3.2. Photocatalytic oxidation performance of as-prepared catalysts

N_2 adsorption–desorption measurement was performed to determine the specific surface area and pore size distribution of the samples. As shown in Table S2 and Fig. S5, these obtained catalysts mainly exhibited type-IV with H4 hysteresis. Pore size distribution (Fig. 3a) showed that the pore size of composite catalysts gradually changed from micropore to mesopore with the decrease of nano-porous carbon component. Moreover, it was clear that the specific surface area (S_{BET} = 271 $m^2 \bullet g^{-1}$)

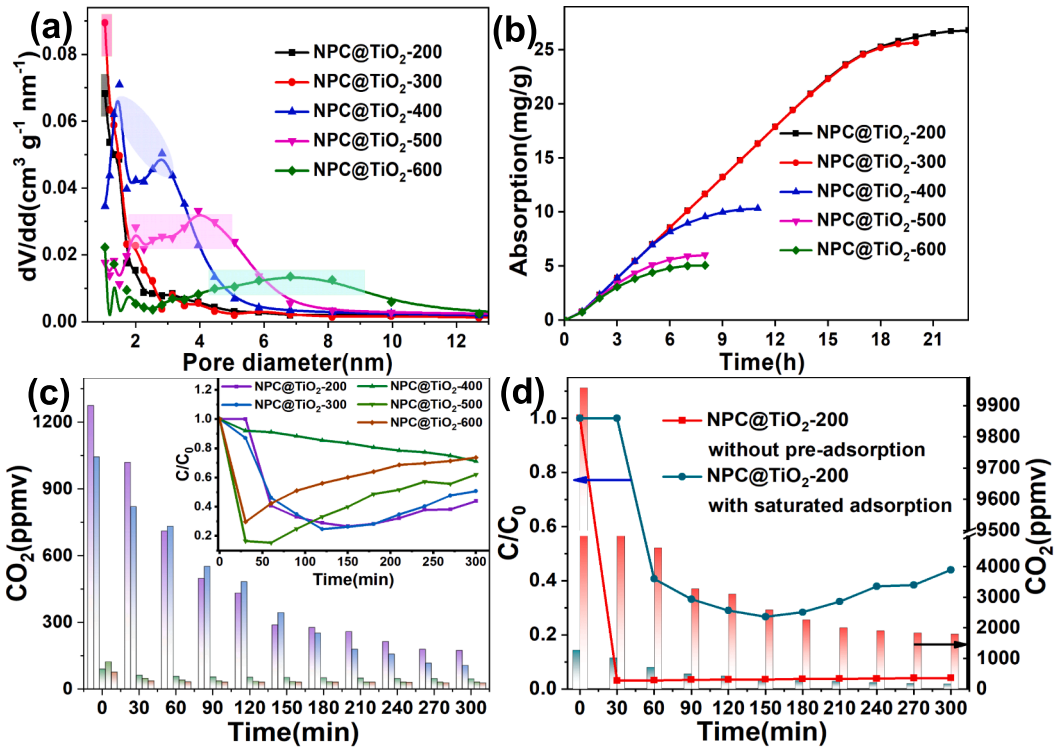

Fig. 3. Pore size distribution (a), toluene adsorption (b), and photocatalytic performance (c) of as-prepared NPC@TiO_2 with saturated toluene adsorption, comparison of photocatalytic activities in NPC@TiO_2-200 and without pre-adsorption (d).

and pore volume ($V = 1.181$ $cm^3 \bullet g^{-1}$) of NPC@TiO_2-200 demonstrated a larger value in comparison to other samples (NPC@TiO_2-600 only displayed a 64.57 $m^2 \bullet g^{-1}$ of S_{BET} and 0.136 $cm^3 \bullet g^{-1}$), which was attributed to the high component of nano-porous carbon and high dispersion of TiO_2 nanocrystal.

Firstly, the toluene-adsorption test was performed using a continuous flow mode. As shown in Fig. 3b, NPC@TiO_2-200 presented a 26.8 $mg \bullet g^{-1}$ of toluene adsorption capacity, which was higher that of other composites with lower nano-porous carbon component, suggesting that nano-porous carbon providing more adsorption active sites for toluene capture due to its higher specific surface area and pore volume[24]. Further, the photocatalytic performance of NPC@TiO_2 with saturated toluene adsorption (NPC@TiO_2-200-WSTA) was evaluated under the simulated sunlight. According to the results of Fig. 3c, it was clearly seen that the degradation as well as the mineralization efficiency were gradually enhanced with the increase of the nano-porous carbon component, and the high-level photocatalytic activity was obtained by NPC@TiO_2-200. This was mainly attributed to the positive contribution of nano-porous carbon for interfacial electron transfer and toluene adsorption trapping[10,42]. However, the sustained degradation and mineralization efficiency of these photocatalysts were generally low under the condition of saturated toluene adsorption, and the highest values obtained by NPC@TiO_2-200 were only 56 % and 174 ppmv of CO_2, and their stabilities of the catalysts gradually decreased with the extension of reaction time. According to our previous reports, the decreased performance of these photocatalysts could be attributed to the accumulation of large amounts of carbonaceous byproducts, leading to the occupation of the adsorption and reaction active sites over the catalysts[6]. In other words, the reservoir effect of nano-porous carbon was significantly inhibited under the saturated toluene adsorption, and eventually resulting in the gradual deactivation of these catalysts.

Interestingly, a higher photocatalytic activity with a 96 % of degradation and 1799 ppmv of CO_2 yield without other gaseous products were obtained when the NPC@TiO_2-200 composite was directly photocatalyzed without saturated toluene adsorption (NPC@TiO_2-200-WOSTA) under the same catalytic conditions (Fig. 3d). The enhanced photocatalytic performance was mainly attributed to the reservoir effect of nano-porous carbon in NPC@TiO_2-200. On the one hand, nano-porous carbon can be used as an efficient toluene adsorption reservoir, effectively promoting the adsorption, reaction, and mass transfer of toluene between TiO_2 shell and nano-porous carbon core, so as to avoid the accumulation of high-boiling intermediates [6,14]. On the other hand, as an effective electron reservoir, nano-porous carbon could also promote the formation of interfacial oxidation free radicals by improving photogenerated charge separation, and subsequently enhanced the deep oxidation of interfacial conversion products [14]. Therefore, avoiding the saturated adsorption of toluene on the NPC@TiO_2 to guarantee the reservoir effect of nano-porous carbon is the key factor to maintain the high activity and stability of the photocatalyst.

3.3. *Synergetic anti-deactivation mechanism of NPC core and TiO_2 shell*

To further clarify the synergic anti-deactivation mechanism of nano-porous carbon core and anatase TiO_2 shell, the in-situ DRIFTS were employed to analyze the changes of oxidation products at the interface of the photocatalyst. The toluene adsorption analysis of in-situ DRIFTS (see SI in Fig. S6) showed that the typical functional groups of –CH, $–CH_3$ and C=C were appeared at 2820 and 1340 cm^{-1}, 2730 cm^{-1}, 1690 and 1590 cm^{-1}, respectively, which were assigned to the characteristic peaks of toluene. Among them, the peak intensity of C=C and –CH are obviously strong, indicating that a tighter adsorption pattern between C=C and –CH of the benzene ring with the composite interfaces may be formed, and the peak intensity of $–CH_3$ is relatively weak. The above results suggested that there were various adsorption forms of toluene on the composite interface, and the benzene ring structure could form a more stable adsorption pattern with the adsorption interfaces[10]. The characteristics of oxidation morphology of toluene was further recorded and investigated by in-situ DRIFTS (see Fig. 4a and 4b). During the photocatalytic oxidation of toluene, hydroxyl radicals attacked the

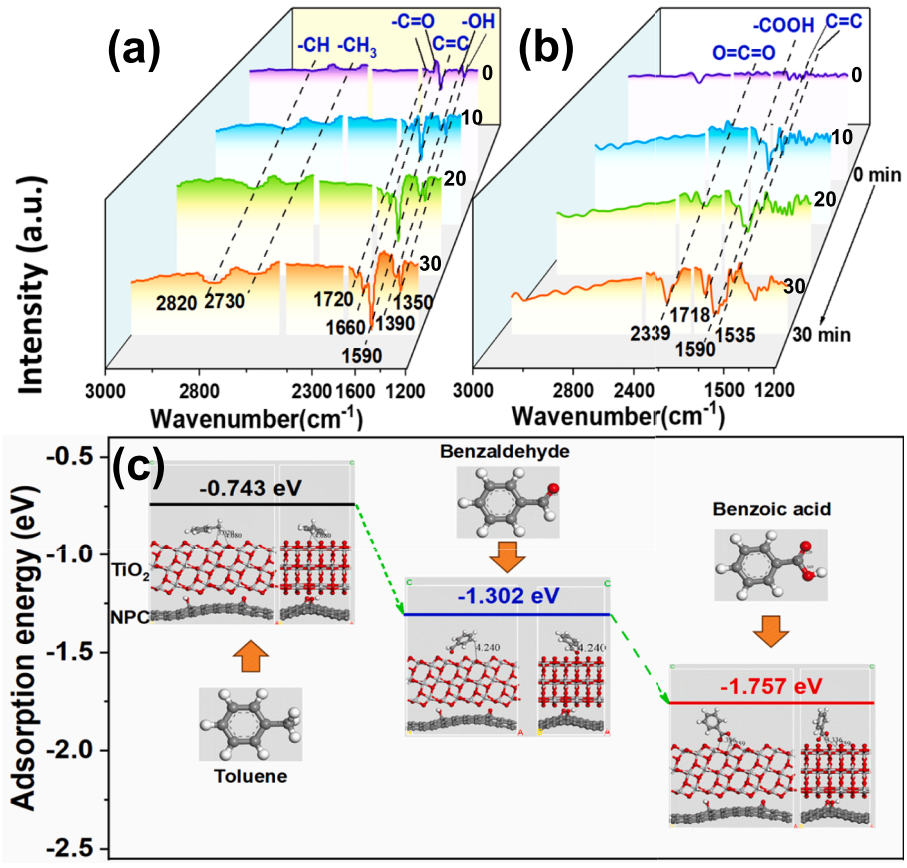

Fig. 4. In-situ DRIFTS of photocatalytic oxidation of toluene with toluene pre-adsorption (a) and without toluene pre-adsorption (b) over NPC@TiO_2 under simulated sunlight. Adsorption energy of toluene and its main byproducts (benzaldehyde and benzoic) on NPC@TiO_2 based on DFT calculation (c).

methyl group of toluene, and subsequently led to the formation of byproducts such as benzaldehyde and benzoic acid (See SI in Table S3 and Fig. S7)[20]. As shown in Fig. 4a, the typical peaks of –C=O (1660 and 1720 cm^{-1}) and –OH (1390 and 1350 cm^{-1}) were observed at the interface of NPC@TiO_2 with toluene pre-adsorption, which were assigned to the characteristic peaks of benzaldehyde and benzoic acid [20]. In addition, the characteristic peaks such as –CH (2820 cm^{-1}), $–CH_3$ (2730 cm^{-1}), C=C (1660 and 1590 cm^{-1}) were also observed, which could be assigned to the characteristic peaks of adsorbed toluene. This was also observed from the in-situ DRIFTS of NPC@TiO_2-300 ~ 400 with toluene pre-adsorption (See SI in Fig. S8). These results suggest that there was a competitive oxidation state between toluene and its oxidation products under toluene pre-adsorption, which means the composite interface cannot produce enough oxidation radicals in time to promote the oxidation decomposition of toluene and further mineralization of the carbonaceous intermediates. Fig. 4b shows the in-situ DRIFTS of toluene photocatalytic oxidation on NPC@TiO_2 without toluene pre-adsorption. It is interesting to note that the characteristic peak of toluene was not observed at the catalyst interface, only the obvious characteristic peak of O=C=O (2339 cm^{-1}) and the weak peaks of –COOH (1718 cm^{-1}) and C=C (1590 and 1535 cm^{-1}) were appeared in the spectra, which was assigned to the characteristic peaks of CO_2 and a small amount of benzoic acid. This means that there is no competitive oxidation between toluene and its oxidation products on the catalyst interface, and the catalyst interface without toluene pre-adsorption can produce enough oxidation radicals to realize the deep oxidation of toluene. The results further confirm that carbonaceous deposits can be significantly suppressed by maintaining the reservoir effect of the photocatalyst. Thus, the interfacial activity of catalyst can be maintained, and the deep oxidation of toluene can be effectively promoted.

To further estimate the adsorption strength of carbonaceous intermediates on NPC@TiO_2, the adsorption energy of toluene and its main oxidation intermediates (such as benzaldehyde and benzoic acid) were explored by DFT calculations. The adsorption behavior of toluene and its oxidation intermediates on the catalyst surface is predominantly governed by interfacial chemistry and functional group interactions at the active sites (such as hydrophobic π-π interactions of NPC, Lewis acid sites of Ti^{4+}). As shown in Fig. 4c, the adsorption energy of toluene, benzaldehyde, and benzoic acid on NPC@TiO_2 are calculated to be −0.743, −1.302, −1.757 eV, respectively. Obviously, these oxidative intermediates are more strongly adsorbed on NPC@TiO_2 surface than toluene and some of them can be further transformed into high-boiling products (with higher molecular weight) [6,8,20]. The strong interaction between recalcitrant carbonaceous intermediates and the catalyst surface would decrease the number of active sites, which is the main reason for the photocatalyst deactivation. The adsorption energy of these three compounds on TiO_2 and nano-porous carbon was also calculated and shown in Fig. S9 and Fig. S10. It is found that the adsorption energy of toluene, benzaldehyde, and benzoic acid on TiO_2 and nano-porous carbon is gradually raised as well. Thereinto, the adsorption energy of these three compounds on nano-porous carbon and NPC@TiO_2 is higher than that of TiO_2, which indicates that the synergistic interaction between nano-porous carbon and TiO_2 generates additional active sites for toluene adsorption, particularly at electron-enriched carbon regions near TiO_2 interfaces, thereby significantly promoting toluene adsorption, surface reactions, and mass-transfer. This could effectively slow down the occupation of TiO_2 active sites and avoid the rapid deactivation of the NPC@TiO_2 catalyst.

To estimate the number of carbonaceous species deposited on the photocatalyst surface, the TGA, GC–MS and XPS semi-quantitative method (Fig. 5) were employed to analyze the relative content of the main surface composition and state on different used NPC@TiO_2

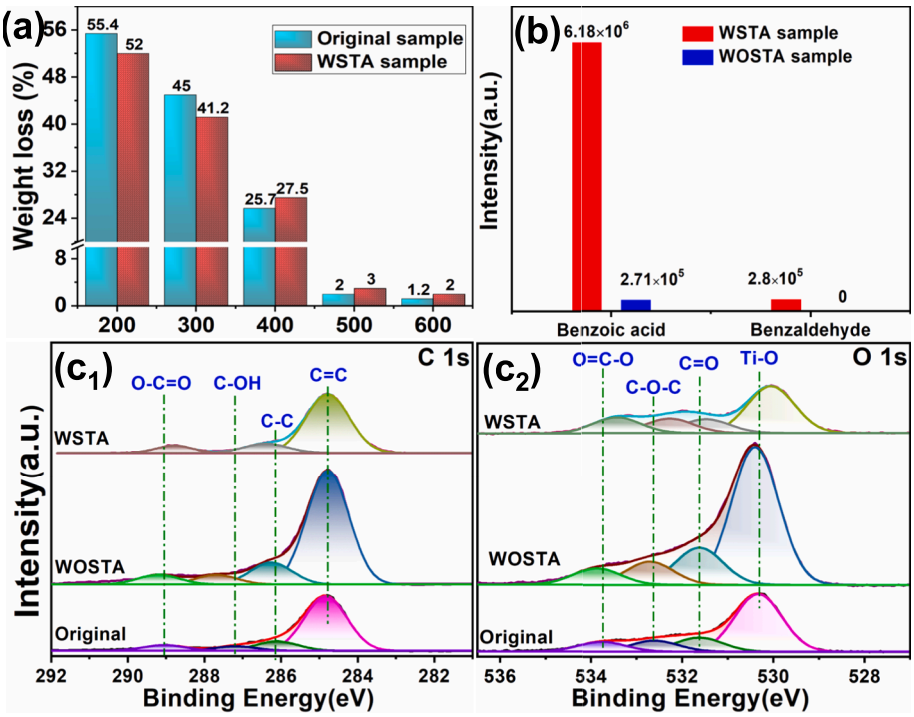

Fig. 5. Weight loss (a) of as-prepared NPC@TiO_2 (different activated temperature). Relative content (b) of main intermediates on NPC@TiO_2 with and without saturated toluene adsorption. High-resolution XPS of C1s (c_1) and O1s (c_2) on NPC@TiO_2-200-WSTA and NPC@TiO_2-200-WOSTA after photocatalytic reaction, and original NPC@TiO_2-200.

composites. The relative weight loss (W_{WSTA}-$W_{original}$) between WSTA sample and original sample were calculated to be −3.4 % (NPC@TiO_2-200), −3.8 % (NPC@TiO_2-300), 1.8 % (NPC@TiO_2-400), 1.0 % (NPC@TiO_2-500) and 0.8 % (NPC@TiO_2-600) (Fig. 5a). This clearly indicates less carbonaceous deposits were formed on NPC@TiO_2 with high content of nano-porous carbon than that of with low content of nano-porous carbon. It is noted that the NPC@TiO_2-200 and NPC@TiO_2-300 display negative value as compared with others, which can be attributed to the decomposition of pre-existing unstable carbonaceous species. This is also can be seen from the HR-TEM analysis of the used NPC@TiO_2-200 (See SI in Fig. S11). As shown in Fig. S11a-c, it can be clearly seen that the internal structure of the NPC@TiO_2 photocatalyst was changed from Core-Shell structure to Yolk-Shell structure. According to the EDX data (See SI in Fig. S11d and Table S4), the corresponding element mapping of the used NPC@TiO_2-200 shows the typical Yolk (carbon core)-Shell (TiO_2 shell) structure, where the proportion of C element decreases from 88.25 % to 28.38 %, O element increases from 9.89 % to 27.80 %, and Ti element increases from 1.86 % to 43.82 %. Due to this transformation to multi-interface structure, more active sites of the photocatalyst can be exposed during the photocatalysis process, and further improve the adsorption and capture, mass transfer and deep oxidation of toluene.

As shown in Fig. 5b, the amounts of the main byproducts (benzaldehyde and benzoic acid) on NPC@TiO_2-200 with saturated toluene adsorption (NPC@TiO_2-200-WSTA) were significantly higher than that of NPC@TiO_2-200 without saturated toluene adsorption (NPC@TiO_2-200-WOSTA) based on the relative peak area (see SI in Fig. S7). In addition, the proportions of total C, O, and Ti in NPC@TiO_2-200-WSTA, NPC@TiO_2-200-WOSTA and original NPC@TiO_2-200 were calculated to be 32.94 %, 27.86 % and 29.98 % (total C), 39.81 %, 38.28 % and 37.45 % (total O), 27.25 %, 33.86 % and 32.57 % (total Ti), respectively, according to the high-resolution XPS spectra (Fig. 5c1, c2 and Table S5). It is noted that the proportion of total C and O in NPC@TiO_2-200-WSTA is high than that of NPC@TiO_2-200-WOSTA and original NPC@TiO_2-200, which further confirms that more carbonaceous deposits were formed NPC@TiO_2-200-WSTA rather than NPC@TiO_2-200-WOSTA. This is mainly because when the NPC@TiO_2 photocatalyst reaches saturated toluene adsorption, the adsorption reservoir will be in a relatively saturated state. At the initial stage of the photocatalytic reaction, large amounts of adsorbed toluene were rapidly reacted with numerous interface free radicals, and the excess depletion of free radicals and the formation of carbonaceous deposits will severely inhibit the reservoir effect of the photocatalyst, resulting in a decrease in toluene capture efficiency and free radical formation efficiency, and eventually the gradual deactivation of the photocatalyst.

TiO_2 photocatalyst deactivation has been observed with various VOCs[43–45]. However, the degree of deactivation not only depend on the kind of VOCs, but also the disposal method of VOCs before photocatalytic reaction. In particular, the saturated toluene adsorption induces severe deactivation as demonstrated in this study. As described in Fig. 6, due to the inefficient reservoir effect of conventional TiO_2 photocatalyst, the degradation of VOCs often leaves recalcitrant carbonaceous residues on the photocatalyst surface because of incomplete degradation, which causes the catalyst deactivation[6,18,46]. The core–shell structure composed of nano-porous carbon (NPC) and TiO_2 significantly enhances the photocatalytic “reservoir effect”. This synergistic architecture operates through three key mechanisms: (1) Electron conduction & radical generation, NPC serves as an efficient electron acceptor due to its superior charge transport properties, facilitating rapid electron transfer from the TiO_2 interface. This process not only suppresses charge recombination but also accelerates the generation of oxidizing radicals (e.g., •OH, $\bullet O_2^-$), thereby enhancing photocatalytic activity. (2) Adsorption-enriched catalysis, with its high specific surface area and strong VOC adsorption affinity, NPC acts as a selective molecular trap, concentrating target pollutants near active sites. This localized enrichment prevents VOC escape and ensures a continuous supply of reactants for interfacial oxidation. (3) Intermediate migration & stability enhancement, the organic affinity of NPC promotes the diffusion of reaction intermediates away from TiO_2 active sites. This mitigates the accumulation of carbonaceous deposits, reducing active

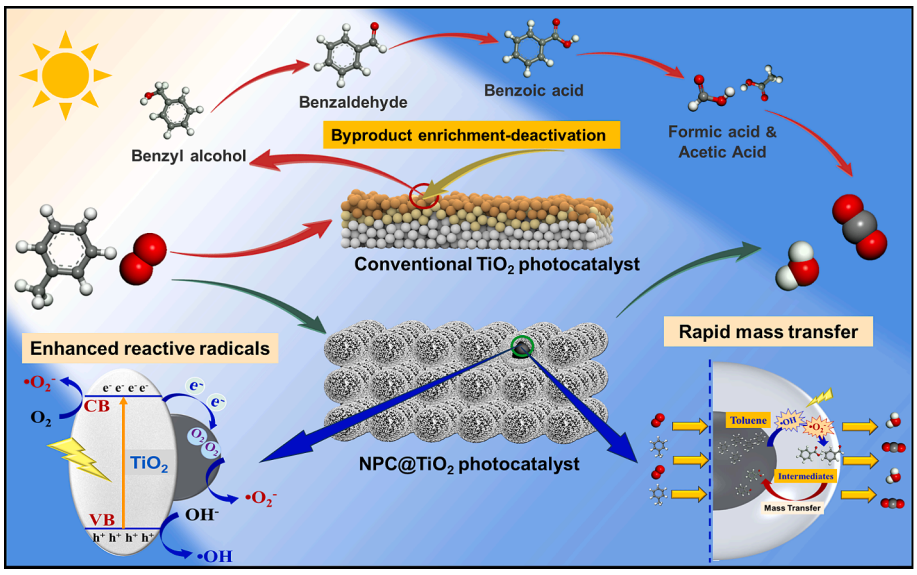

Fig. 6. Enhanced photocatalytic oxidation mechanism of toluene over NPC@TiO_2.

site blockage and thus preserving long-term catalytic stability. Thus, the performance of this system is highly dependent on maintaining effective reservoir functionality. Once the reservoir effect of the photocatalyst is inhibited, such as the saturation adsorption of toluene, the diminished adsorption capacity leads to a sharp decline in both pollutant trapping efficiency and radical generation rates. Consequently, sustaining optimal reservoir capacity is essential for ensuring stable and efficient photocatalytic degradation.

4. Conclusions

The deactivation of photocatalyst has been the most serious problem in commercializing this technology. The incomplete oxidation of VOCs often leaves recalcitrant carbonaceous residues on the photocatalyst surface, which causes the catalyst deactivation. This study demonstrated that nano-porous carbon in NPC@TiO_2 as a temporary reservoir of toluene and lone electrons to enhance the selective adsorption trapping of toluene and the separation of photogenerated carrier, thereby reduce the shielding effect of carbonaceous species on the active sites and avoiding the deactivation of catalyst. In addition, in order to decrease the accumulation of carbonaceous by-products on the photocatalyst, effectively avoiding the saturation adsorption of VOCs on the photocatalyst is key factor to ensure the stability of its degradation activity.

Declaration of competing interest

The authors declare that they have no known competing financial interests or personal relationships that could have appeared to influence the work reported in this paper.

Acknowledgements

The authors thank the National Key Research and Development Project of China (2024YFE0110800), National Natural Science Foundation of China (42477411, 22076028 and 42377099), National Key Research and Development Project of China (2023YFC3708203), Guangdong Provincial Key R&D Program (2022-GDUT-A0007), Local Innovative and Research Teams Project of Guangdong Pearl River Talents Program (2017BT01Z032). Many thanks to Xian Qiu who helped to improve the language' accuracy and coherence of our essay.

Appendix A. Supplementary data

Supplementary data to this article can be found online at https://doi.org/10.1016/j.seppur.2025.133016.

Data availability

Data will be made available on request.

References

[1] C. Wang, W. Wang, S. Shao, W. Deng, C. Wang, X. Liu, H. Li, M. Wen, X. Zhang, G. Li, T. An, Occurrence of BTX and PAHs in underground drinking water of coking contaminated sites: Linkage with altitude and health risk assessment by boiling-modified models, Sci. Total Environ. 917 (2024) 170407.
[2] M. Wen, W. Deng, J. Huang, S. Zhang, Q. Lin, C. Wang, S. Ma, W. Wang, X. Zhang, G. Li, T. An, Atmospheric VOCs in an industrial coking facility and the surrounding area: Characteristics, spatial distribution and source apportionment, J. Environ. Sci. 138 (2024) 660–670.
[3] W. Qu, P. Wang, M. Gao, J.-Y. Hasegawa, Z. Shen, Q. Wang, R. Li, D. Zhang, Delocalization Effect Promoted the Indoor Air Purification via Directly Unlocking the Ring-Opening Pathway of Toluene, Environ. Sci. Tech. 54 (2020) 9693–9701.
[4] C. Liang, C. Li, Y. Zhu, X. Du, C. Yao, Y. Ma, J. Zhao, Recent advances of photocatalytic degradation for BTEX: Materials, operation, and mechanism, Chem. Eng. J. 455 (2023) 140461.
[5] X. Yu, C. Zhou, Z. Huang, C. Xin, Y. Lin, F. Fu, S. Li, W. Zhang, Rational design of AgCl@Zr^{3+}-ZrO_2 nanostructures for ultra-efficient visible-light photodegradation of emerging pollutants, Appl Catal B 325 (2023) 122308.
[6] W.P. Zhang, G.Y. Li, H.L. Liu, J.Y. Chen, S.T. Ma, M.C. Wen, J.J. Kong, T.C. An, Photocatalytic degradation mechanism of gaseous styrene over Au/TiO_2@CNTs: Relevance of superficial state with deactivation mechanism, Appl Catal B 272 (2020) 118969.
[7] Z. Chen, Y. Peng, J. Chen, C. Wang, H. Yin, H. Wang, C. You, J. Li, Performance and Mechanism of Photocatalytic Toluene Degradation and Catalyst Regeneration by Thermal/UV Treatment, Environ. Sci. Tech. 54 (2020) 14465–14473.
[8] F. He, U. Muliane, S. Weon, W. Choi, Substrate-specific mineralization and deactivation behaviors of TiO_2 as an air-cleaning photocatalyst, Appl Catal B 275 (2020) 119145.
[9] Y. Tulebekov, Z. Orazov, B. Satybaldiyev, D.D. Snow, R. Schneider, B. Uralbekov, Reaction Steps in Heterogeneous Photocatalytic Oxidation of Toluene in Gas Phase—A Review, Molecules 28 (2023) 6451.
[10] W. Zhang, G. Li, H. Yin, K. Zhao, H. Zhao, T. An, Adsorption and desorption mechanism of aromatic VOCs onto porous carbon adsorbents for emission control and resource recovery: recent progress and challenges, Environ. Sci. Nano 9 (2022) 81–104.
[11] J. Li, X.a. Dong, G. Zhang, W. Cui, W. Cen, Z. Wu, S.C. Lee, F. Dong, Probing ring-opening pathways for efficient photocatalytic toluene decomposition, Journal of Materials Chemistry A, 7 (2019) 3366-3374.
[12] S. Yuan, X. Bao, M. Chen, X. Qin, X. Chen, J. Zhang, C. Zhang, Unravelling the pathway determining the CO_2 selectivity in photocatalytic toluene oxidation on TiO_2 with different particle size, Chem. Eng. J. 470 (2023) 144138.

[13] B. Liu, B. Zhang, B. Liu, Z. Hu, W. Dai, J. Zhang, F. Feng, B. Lan, T. Zhang, H. Huang, Surface Hydroxyl and Oxygen Vacancies Engineering in ZnSnAl LDH: Synergistic Promotion of Photocatalytic Oxidation of Aromatic VOCs, Environ. Sci. Tech. 58 (2024) 4404–4414.
[14] W. Zhang, G. Li, H. Liu, J. Chen, S. Ma, T. An, Micro/nano-bubble assisted synthesis of Au/TiO_2@CNTs composite photocatalyst for photocatalytic degradation of gaseous styrene and its enhanced catalytic mechanism, Environmental Science-Nano 6 (2019) 948–958.
[15] J.Y. Chen, Z.G. He, Y.M. Ji, G.Y. Li, T.C. An, W. Choi, •OH radicals determined photocatalytic degradation mechanisms of gaseous styrene in TiO_2 system under 254 nm versus 185 nm irradiation: Combined experimental and theoretical studies, Appl. Catal. b: Environ., 257 (2019) 117912.
[16] L. Peng, H. Wang, G. Li, Z. Liang, W. Zhang, W. Zhao, T. An, Bioinspired artificial spider silk photocatalyst for the high-efficiency capture and inactivation of bacteria aerosols, Nat. Commun. 14 (2023) 2412.
[17] S. Weon, E. Choi, H. Kim, J.Y. Kim, H.-J. Park, S.-M. Kim, W. Kim, W. Choi, Active 001 facet exposed TiO2 nanotubes photocatalyst filter for volatile organic compounds removal: From material development to commercial indoor air cleaner application, Environ. Sci.tech., 52 (2018) 9330–9340.
[18] S. Weon, F. He, W. Choi, Status and challenges in photocatalytic nanotechnology for cleaning air polluted with volatile organic compounds: visible light utilization and catalyst deactivation, Environ. Sci. Nano 6 (2019) 3185–3214.
[19] H. Li, B. Bharti, V. Manikandan, M.S. AlSalhi, N.N. Asemi, Y. Wang, W. Jin, F. Ouyang, Nitrogen–Fluorine co-doped TiO_2/SiO_2 nanoparticles for the photocatalytic degradation of acrylonitrile: Deactivation and regeneration, Chemosphere 340 (2023) 139986.
[20] S. Weon, W. Choi, TiO_2 Nanotubes with Open Channels as Deactivation-Resistant Photocatalyst for the Degradation of Volatile Organic Compounds, Environ. Sci. Tech. 50 (2016) 2556–2563.
[21] S. Cao, X. Fei, Y. Wen, Z. Sun, H. Wang, Z. Wu, Bimodal mesoporous TiO_2 supported Pt, Pd and Ru catalysts and their catalytic performance and deactivation mechanism for catalytic combustion of Dichloromethane (CH2Cl2), Appl. Catal. A 550 (2018) 20–27.
[22] J. Tang, M. Fu, Y. Mao, S. Yang, W. Lin, Y. Yu, S. Song, Decorating 0 0 1 TiO2 nanosheets on hydrophobic NaY zeolite: An efficient deactivation-resistant photocatalyst for gaseous toluene removal, Chem. Eng. J. 472 (2023) 144883.
[23] H. Liao, H. Xu, X. Zhang, W. Dai, Z. Zhang, Stable bidentate coordination sulfated TiO_2 for highly durable photocatalytic degradation of gaseous acetone, Appl. Catal. A 657 (2023) 119158.
[24] W. Zhang, X. Wang, H. Pan, X. Zeng, G. Li, H. Liu, J. Kong, H. Zhao, T. An, Experimental and DFT investigations on adsorption–regeneration performance and deactivation mechanism over engineered carbon fiber: role of pore structure and functional groups, Environ. Sci. Nano 10 (2023) 2790–2798.
[25] J. Chen, Z. Zhang, W. Zhu, L. Zhang, B. Zhao, Y. Ji, G. Li, T. An, Superoxide radical enhanced photocatalytic performance of styrene alters its degradation mechanism and intermediate health risk on TiO_2/graphene surface, Environ. Res. 195 (2021) 110747.
[26] X. An, K. Zhao, W. Pang, W. Zhang, L. Wang, T. Guo, D. Fu, Balancing the CO_2 adsorption properties and the regeneration energy consumption via the functional molecular engineering hierarchical pore-interface structure, Chem. Eng. J. 431 (2022) 133877.
[27] K. Zhou, W. Ma, Z. Zeng, R. chen, X. Xu, B. Liu, H. Li, H. Li, L. Li, Waste biomass-derived oxygen and nitrogen co-doped porous carbon/MgO composites as superior acetone adsorbent: Experimental and DFT study on the adsorption behavior, Chemical Engineering Journal, 387 (2020) 124173.
[28] W. Zhang, X. Xiao, L. Zheng, C. Wan, Fabrication of TiO_2/MoS_2@zeolite photocatalyst and its photocatalytic activity for degradation of methyl orange under visible light, Appl. Surf. Sci. 358 (2015) 468–478.
[29] Y. Wang, Y. Zhang, X. zhu, Y. Liu, Z. Wu, Fluorine-induced oxygen vacancies on TiO_2 nanosheets for photocatalytic indoor VOCs degradation, Appl Catal B 316 (2022) 121610.
[30] J. Wang, P. Rao, W. An, J. Xu, Y. Men, Boosting photocatalytic activity of Pd decorated TiO_2 nanocrystal with exposed (001) facets for selective alcohol oxidations, Appl Catal B 195 (2016) 141–148.
[31] Y. Zhang, J.-X. Liu, K. Qian, A. Jia, D. Li, L. Shi, J. Hu, J. Zhu, W. Huang, Structure Sensitivity of Au-TiO_2 Strong Metal–Support Interactions, Angew. Chem. Int. Ed. 60 (2021) 12074–12081.
[32] M. Li, B. Lu, Q.-F. Ke, Y.-J. Guo, Y.-P. Guo, Synergetic effect between adsorption and photodegradation on nanostructured TiO_2/activated carbon fiber felt porous composites for toluene removal, J. Hazard. Mater. 333 (2017) 88–98.
[33] Y. Guo, C. Su, H. Chen, B. Liu, L. Yu, J. Wang, J. Qiu, Z. Zeng, L. Li, Mechanistic effects of graphitization degrees and surface oxygen heteroatoms on VOCs adsorptive separation: Experimental and theoretical perspective, J. Environ. Chem. Eng. 10 (2022) 108985.
[34] W. Zhang, X. Xiao, Y. Li, X. Zeng, L. Zheng, C. Wan, Liquid-exfoliation of layered MoS_2 for enhancing photocatalytic activity of TiO_2/g-C_3N_4 photocatalyst and DFT study, Appl. Surf. Sci. 389 (2016) 496–506.
[35] S. Feizpoor, A. Habibi-Yangjeh, R. Luque, Preparation of TiO_2/Fe-MOF n-n heterojunction photocatalysts for visible-light degradation of tetracycline hydrochloride, Chemosphere 336 (2023) 139101.
[36] J. Huang, L. Dou, J. Li, J. Zhong, M. Li, T. Wang, Excellent visible light responsive photocatalytic behavior of N-doped TiO_2 toward decontamination of organic pollutants, J. Hazard. Mater. 403 (2021) 123857.
[37] M. Jiang, M. Zhang, L. Wang, Y. Fei, S. Wang, A. Núñez-Delgado, A. Bokhari, M. Race, A. Khataee, J. Jaromír Klemeš, L. Xing, N. Han, Photocatalytic degradation of xanthate in flotation plant tailings by TiO_2/graphene nanocomposites, Chem. Eng. J. 431 (2022) 134104.
[38] Y.-L. Zhao, N. Ullah, S. Chen, R.-Q. Zhang, n → π* Interaction Promoted Charge Carrier Transfer between Helical SWNTs and a 4-(1-Pyrenyl)phenyl Group, J. Phys. Chem. C 123 (2019) 13976–13982.
[39] Y. Yu, Q. Zeng, S. Tao, C. Xia, C. Liu, P. Liu, B. Yang, Carbon Dots Based Photoinduced Reactions: Advances and Perspective, Adv. Sci. 10 (2023) 2207621.
[40] K. Wenderich, K. Zhu, Y. Bu, F.D. Tichelaar, G. Mul, A. Huijser, Photophysical Characterization of Ru Nanoclusters on Nanostructured TiO_2 by Time-Resolved Photoluminescence Spectroscopy, J. Phys. Chem. C 127 (2023) 14353–14362.
[41] C. Bai, D. Yang, C. Liu, F. Zhu, C. Tu, G. Li, Y. Luo, In situ synthesis NiO@TiO_2/MXene as a promoter for ammonium perchlorate based solid propellants, Appl. Surf. Sci. 652 (2024) 159228.
[42] F. Dong, H. Wang, Z. Wu, One-Step "Green" Synthetic Approach for Mesoporous C-Doped Titanium Dioxide with Efficient Visible Light Photocatalytic Activity, J. Phys. Chem. C 113 (2009) 16717–16723.
[43] L. Zhang, L. Xue, B. Lin, Q. Zhao, S. Wan, Y. Wang, H. Jia, H. Xiong, Noble Metal Single-Atom Catalysts for the Catalytic Oxidation of Volatile Organic Compounds, ChemSusChem 15 (2022) e202102494.
[44] H. Jia, Y. Xing, L. Zhang, W. Zhang, J. Wang, H. Zhang, W. Su, Progress of catalytic oxidation of typical chlorined volatile organic compounds (CVOCs): A review, Sci. Total Environ. 865 (2023) 161063.
[45] J. Yang, Y. Huang, J. Su, L. Chen, M. Zhang, M. Gao, M. Yang, F. Wang, X. Zhang, B. Shen, Low temperature denitrification and mercury removal of Mn/TiO_2-based catalysts: A review of activities, mechanisms, and deactivation, Sep. Purif. Technol. 297 (2022) 121544.
[46] P. Yao, H. Liu, D. Wang, J. Chen, G. Li, T. An, Enhanced visible-light photocatalytic activity to volatile organic compounds degradation and deactivation resistance mechanism of titania confined inside a metal-organic framework, J. Colloid Interface Sci. 522 (2018) 174–182.